ARTICLES

A linear approach for the evolution of coherent structures in shallow mixing layers

Bram C. van Prooijen and Wim S. J. Uijttewaal

Delft University of Technology, Faculty of Civil Engineering and Geosciences, P.O. Box 5048, 2600 GA Delft, The Netherlands

The development of large coherent structures in a shallow mixing layer is analyzed. The results are validated with experimental data obtained from particle tracking velocimetry. The mean flow field is modeled using the self-similarity of the velocity profiles. The characteristic features of the down-stream development of a shallow mixing layer flow, like the decrease of the velocity difference over the mixing layer, the decreasing growth of the mixing layer width, and the transverse shift of the center of the mixing layer layer are fairly well represented. It turned out that the entrainment coefficient could be taken constant, equal to a value obtained for unbounded mixing layers: $\alpha = 0.085$. Linearization of the shallow water equations leads to a modified Orr–Sommerfeld equation, with turbulence viscosity and bottom friction as dissipative terms. Growth rates are obtained for each position downstream, using the model for the mean flow field. For a given energy density spectrum at the inflow boundary, integration of the growth rates along the downstream direction yields the spectra at various downstream positions. These spectra provide a measure for the intensity and the length scale of the coherent structures (the dominant mode). The length scales found are in good agreement with the measured ones. The length scale of the most unstable mode appears much larger than the length scale of the dominant mode. Obviously, the longevity of the coherent structures plays a significant role. Three growth regimes can be distinguished: in the first regime the dominant mode is growing, in the second regime the dominant mode is dissipating, but other modes are still growing, and in the third regime all modes are dissipating. It is concluded that the development of the coherent structures in a shallow mixing layer can fairly well be described and interpreted by the proposed linear analysis. © *2002 American Institute of Physics.* [DOI: 10.1063/1.1514660]

I. INTRODUCTION

Rivers, in particular low-land rivers, belong to the class of wide open channel flows. The aspect ratio (depth/width) is on the order of 5% or less. At several places in rivers, shallow mixing layers can arise, i.e., transverse shear layers between contiguous flows of different velocity. Examples are found at the confluence of two rivers,[1] in a compound channel at the interface between the main channel and a flood plain, or between the main channel and a groyne field.[2] Characteristic of these shallow shear flows is the anisotropy of the turbulent motion. The no-slip boundary at the bottom gives rise to a turbulent wall flow, with a characteristic length scale of the order of the water depth. The transverse shear layer can, however, contain length scales much larger than the water depth, resulting in a large scale motion restricted to the horizontal plane. This large scale motion has a significant influence on the transverse exchange of mass and momentum, which is important for example for the dispersion of pollutants and for sediment transport.

The typical length scales can be visualized in an experiment by the injection of dye in the center of a shallow mixing layer. Figure 1 shows large scale coherent structures, to be interpreted as Kelvin–Helmholtz instabilities. The dye band rolls up by the action of large scale motion, whereas the dispersion of dye on smaller scales results in a widening of the dye band.

Due to the difficulties it causes for turbulence modeling, the anisotropy in shallow shear flows has been the subject of many studies,[1,3–7] with emphasis on the interaction between the large scale motion and the small scale motion. The influence of the no-slip wall on the large scale motion is often represented by a bottom friction parameter S, according to Alavian and Chu:[3]

$$S = \frac{c_f}{2} \frac{\delta}{H} \frac{U_c}{\Delta U},\tag{1}$$

with $c_f = \tau_b / \rho \frac{1}{2} U^2$ the bottom friction coefficient, δ the mixing layer width, H the water depth, U_c the velocity in the center of the mixing layer, and ΔU the velocity difference over the mixing layer. This bottom friction parameter is in-

FIG. 1. Large coherent structures are visualized by dye injection in the center of the mixing layer just downstream of the splitter plate. The arrows indicate the velocities in the two undisturbed streams. The width of the flow domain is 3 m and the water depth is 67 mm.
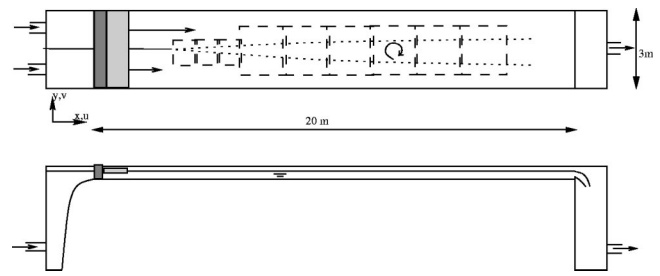

FIG. 2. Schematic top and side view of the shallow flow facility. The mixing layer region is indicated by dotted lines. The measurement areas are indicated by the dashed squares.

II. EXPERIMENTS

A. The flume and flow conditions

Experiments were conducted in a shallow flow facility with a length of 20 m and a width of 3 m, Fig. 2. The inlet section of the flume consists of two parts, each with a separate water supply, in order to establish a velocity difference. The inlet section has a vertical contraction that connects to the horizontal part of the flume. Screens are placed between the contraction and the entrance of the horizontal part to obtain a homogeneous inflow. Floating foam boards are placed just downstream from the screens to suppress surface waves. In order to have a fully developed turbulent boundary layer at the confluence, the flows are initially separated by a 3-m-long thin splitter plate. The horizontal bottom and the sidewalls of the flume consist of glass plates, assuring a smooth surface. A sharp crested weir regulates the outflow.

Two shallow mixing layers are examined (Table I), which are similar to the cases studied by Uijttewaal and Booij,[7] who used laser Doppler anemometry. Here we use particle tracking velocimetry (PTV) as a measurement technique since it yields a dense grid of velocity points. This is advantageous for the determination of high velocity gradients in transverse direction and for a proper determination of the development of the mixing layer width in the downstream direction. The data of this study compare well with the results of Uijttewaal and Booij.[7] The two configurations demonstrate the effect of the water depth on the evolution of the coherent structures. The Reynolds number, based on the mean velocity and the water depth, is sufficiently high (Re >4000) to ensure the flow is fully turbulent and the Froude number sufficiently low (Fr<0.5) to minimize the effects of surface disturbances.

B. Particle tracking velocimetry (PTV)

Particle tracking velocimetry (PTV) is applied to obtain sequences of velocity maps of the surface velocity. Floating polypropylene beads (more than 90% submerged) with a di-

terpreted as a measure of the ratio of dissipation to production of kinetic energy contained in the large eddies. A critical value S_c denotes equilibrium of production and dissipation and lies in the range of 0.06–0.12, confirmed by experiments[1,7] and stability analyses.[4,5] The critical bottom friction number is used to determine the development of the mixing layer width and for the prediction of the presence of large scale motion. However, the critical bottom friction number just indicates the equilibrium of the production and dissipation of kinetic energy, and is not a measure for the amount of kinetic energy. As the advection of kinetic energy plays a role, the growth rate itself is not sufficient for the determination of turbulence characteristics, like the energy density and typical length scale. In this study we aim to determine the development of the coherent structures in the downstream direction, taking into account the effect of advected kinetic energy. For simplicity we consider a mixing layer in a straight horizontal flume without variations in bathymetry or bottom roughness.

The development of the mean flow field is described by a quasi-one-dimensional model, based on self-similarity of the velocity profiles. The development of the properties of the large scale motion is subsequently determined by linear stability analysis, using the calculated mean flow field as base flow. We make use of simplified analyses in order to understand the main mechanisms. The results are validated by experimental data, obtained with particle tracking velocimetry.

TABLE I. Flow conditions at the end of the splitter plate.

	H (mm)	$U_1(x_0)$ [m/s]	$U_2(x_0)$ [m/s]	c_f [-]
I	42	0.25	0.11	0.0064
II	67	0.32	0.13	0.0054

ameter of 2 mm are used as tracers. A distributor is used to spread the beads homogeneously on the water surface. A digital camera mounted on a bridge over the flume recorded the positions of the particles. The camera (Kodak ES1) has a resolution of 1008×1018 pixels with 256 gray levels and a frame rate of 30 Hz. Time series of images are stored directly on the hard disk of a PC to a maximum of 10 000 frames for a single continuous sequence. Measurements are performed for nine connected areas, covering the mixing layer over a length of 11 m, as indicated in Fig. 2. Since the upstream part of the mixing layer contains small details the first three measurement planes have a dimension of 0.82 m$\times$0.82 m to obtain a resolution sufficiently high to resolve the relatively small coherent structures. The last six areas have dimensions of 1.65 m$\times$1.65 m to capture the full mixing layer width. Typically 2500 particles were detected per image. The large scale motion can therefore be captured, but the small scale turbulence is not fully resolved. A PTV-algorithm[8] is used to determine the velocity of the individual particles. This method tracks the paths of individual particles and calculates the velocity, resulting in an unstructured velocity map. Interpolation of the velocity vectors yields a sequence of velocity maps on a structured grid.

III. MODELING

The modeling of the development of the coherent structures in a shallow mixing layer is done in two steps. First the mean flow field is determined using a quasi-one-dimensional model, based on self-similarity. Second, a linear stability analysis is performed to predict the development of the coherent structures for the given base flow. This procedure assumes that the influence of the coherent structures on the mean flow is already accounted for in the quasi-one-dimensional model. Both models are based on the shallow water equations, which are described first.

A. Shallow water equations

The shallow water equations form the basis of the modeling of the mean flow field and the linear stability analysis. As the horizontal length scales are significantly larger than the water depth the flow is described by the two-dimensional shallow water equations (the De Saint Venant equations). The continuity equation and the momentum equations in the horizontal plane are integrated over the water depth and averaged over a period larger than the time scale of the three-dimensional bottom turbulence, but smaller than the time scale of the large scale motion, resulting in: continuity,

$$\frac{\partial \tilde{h}}{\partial t} + \frac{\partial \tilde{h}\tilde{u}}{\partial x} + \frac{\partial \tilde{h}\tilde{v}}{\partial y} = 0; \tag{2}$$

x momentum,

$$\frac{\partial \tilde{u}}{\partial t} + \tilde{u}\frac{\partial \tilde{u}}{\partial x} + \tilde{v}\frac{\partial \tilde{u}}{\partial y} = -g\frac{\partial \tilde{h}}{\partial x} - \frac{c_f}{2\tilde{h}}\tilde{u}\sqrt{\tilde{u}^2 + \tilde{v}^2} + \nu_t \nabla^2 \tilde{u}; \tag{3}$$

y momentum:

$$\frac{\partial \tilde{v}}{\partial t} + \tilde{u}\frac{\partial \tilde{v}}{\partial x} + \tilde{v}\frac{\partial \tilde{v}}{\partial y} = -g\frac{\partial \tilde{h}}{\partial y} - \frac{c_f}{2\tilde{h}}\tilde{v}\sqrt{\tilde{u}^2 + \tilde{v}^2} + \nu_t \nabla^2 \tilde{v}, \tag{4}$$

where u is the velocity in streamwise direction x, and v the velocity in lateral direction y of the horizontal plane. The depth-and-short-time-average operator is denoted by a tilde ($\sim$). The bed friction coefficient c_f for turbulent flow is determined over a smooth bottom by

$$\frac{1}{\sqrt{\frac{1}{2}c_f}} = \frac{1}{\kappa}\left[\ln\left(\mathrm{Re}\sqrt{\frac{1}{2}c_f}\right) + 1\right], \tag{5}$$

where $\mathrm{Re}(=UH/\nu)$ denotes the depth-based Reynolds number. Since we aim to "resolve" the large scale coherent motion the turbulence to be modeled as an effective eddy viscosity ν_t is restricted to the small-scale turbulence, produced in the bottom boundary layer (see also Chen and Jirka[4]). The small scale bottom turbulence is estimated here by using a simple expression for the turbulence eddy viscosity, see, for example, Fisher et al.:[9]

$$\nu_t = 0.15 H u_*. \tag{6}$$

This definition differs from the approach of Alavian and Chu,[3] who used an eddy viscosity based on the large scale motion, using the mixing layer width and the velocity difference over the mixing layer, which resulted in a higher eddy viscosity.

B. Mean flow field

In order to determine the base flow for the stability analysis, an analytical model is formulated to predict the mean streamwise velocity field. For the determination of the mean velocity, the influence of the small scale bottom turbulence is neglected, i.e., the eddy viscosity ν_t is set to zero. A characteristic property of an unbounded plane mixing layer is the self-similarity of the transverse profile of the streamwise velocity.[10] This self-similarity is also found for shallow mixing layers, according to the current and previous experiments.[1,7] Characteristic properties of the shallow mixing layer are: the downstream decrease of the velocity difference, the decreasing growth rate of the mixing layer width, and the shift of the center of the mixing layer to the low velocity side. A model for the mean flow field should capture all these properties.

The flow outside the mixing layer defines the mean velocity difference over the mixing layer ($\Delta U = U_1 - U_2$) and the mean velocity in the center of the mixing layer ($U_c = (U_1 + U_2)/2$). The width of the mixing layer (δ) is defined here by the ratio of the velocity difference ΔU and the lateral gradient of the velocity in the center ($\partial U/\partial y_c$):

$$\delta = \frac{\Delta U}{\dfrac{\partial U}{\partial y_c}}. \tag{7}$$

Self-similarity implies that the transverse profiles of the streamwise velocity can be described by a profile function. A
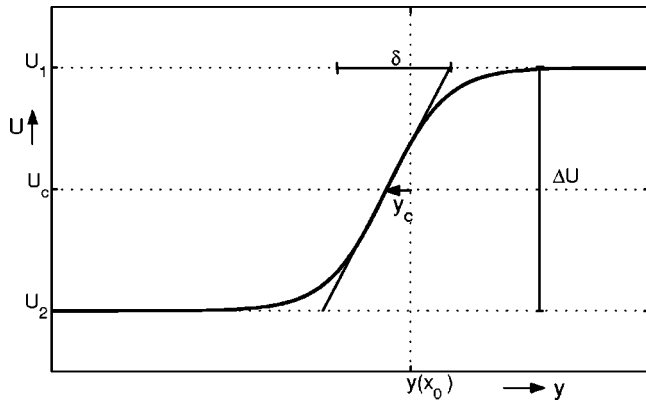
FIG. 3. Sketch of the lateral profile of the stream wise velocity, according to Eq. (8).
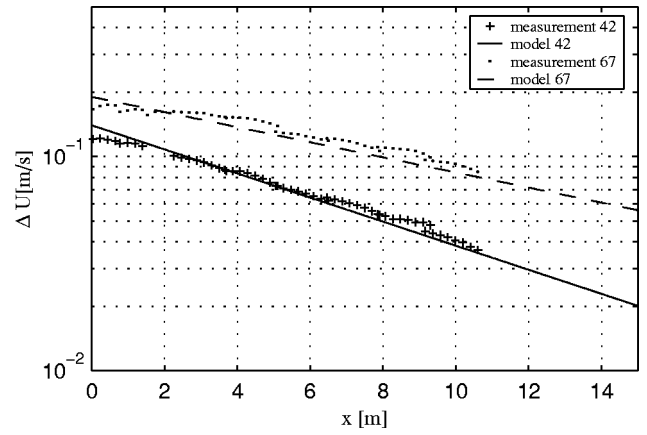

FIG. 4. Development of the velocity difference $\Delta U(x)$ in streamwise direction for the 42 and 67 mm cases according to the measurements and the model, Eq. (12).

variety of functions can be considered, e.g., the error function or the hyperbolic tangent. We use the hyperbolic tangent (tanh), because it fits the data well. The exact shape turned out to affect the results of this analysis only weakly. The mean flow field is then approximated by (see the sketch in Fig. 3)

$$U(x,y)=U_c(x)+\frac{\Delta U(x)}{2}\tanh\left(\frac{y-y_c(x)}{\frac{1}{2}\delta(x)}\right). \qquad (8)$$

By using a profile function the two-dimensional formulation is reduced to a formulation depending on the downstream position (x) only. The development of the velocity difference ΔU, the velocity in the center of the mixing layer U_c, the transverse position of the center of the mixing layer y_c, and the mixing layer width δ will be specified in the following.

The velocity in the center of the mixing layer is approximated by a constant, U_c. This assumption is justified by using the incompressibility condition. The discharge at the inlet section should be equal to the discharge far downstream:

$$U_1(x_0)\frac{HW}{2}+U_2(x_0)\frac{HW}{2}=U(x_\infty)HW, \qquad (9)$$

with W denoting the width of the flow domain, H the constant water depth, $U_1(x_0)$ and $U_2(x_0)$ the initial streamwise velocities outside the mixing layer, and U_∞ the uniform velocity far downstream. This leads to $U(x_\infty)=(U_1(x_0)+U_2(x_0))/2=U_c$. In the experiments, U_c shows a slight increase ($<3\%$) in downstream distance due to the free-surface slope and the horizontal bottom.

The velocities outside the mixing layer are not influenced by the mixing layer. These flows can be considered to be one-dimensional. The development of the velocity difference $\Delta U(x)$ is then determined by the momentum equation in streamwise direction[1] [Eq. (3)] for the high velocity side, denoted by the index 1, and the low velocity side, denoted by the index 2:

$$\frac{1}{2}\frac{dU_1^2}{dx}+\frac{c_{f_1}}{2H_1}U_1^2+g\frac{dH_1}{dx}=0, \qquad (10)$$

$$\frac{1}{2}\frac{dU_2^2}{dx}+\frac{c_{f_2}}{2H_2}U_2^2+g\frac{dH_2}{dx}=0. \qquad (11)$$

The streamwise gradient of the water level is the same for both sides as demonstrated in previous experiments.[7] After subtraction of Eq. (11) from Eq. (10), using $c_f\equiv c_{f_c}\simeq(c_{f_1}+c_{f_2})/2$, and using a constant U_c, the velocity difference $\Delta U(x)$ is expressed by

$$\Delta U(x)=\Delta U_0\exp\left(-\frac{c_f}{h}x\right), \qquad (12)$$

where ΔU_0 denotes the velocity difference at the inflow. The predicted exponential decrease of the velocity difference is in good agreement with the measurements as shown in Fig. 4.

In an unbounded self-preserving mixing layer the spreading rate, i.e., the growth of the mixing layer width $\delta(x)$, is proportional to the relative velocity difference:

$$\frac{d\delta}{dx}=\alpha\frac{\Delta U(x)}{U_c}. \qquad (13)$$

The entrainment coefficient α has an empirically determined value of $\alpha\simeq0.085$ for undisturbed unbounded mixing layers, based on numerous independent experiments.[11] Substitution of the velocity difference ΔU from Eq. (12) and integration over x leads to

$$\delta(x)=\alpha\frac{\Delta U_0}{U_c}\frac{h}{c_f}\left(1-\exp\left(-\frac{c_f}{h}x\right)\right)+\delta_0. \qquad (14)$$

The initial width δ_0 is imposed by the thickness of the boundary layers that have developed on both sides of the splitter plate and is approximately $\delta_0\simeq h$. The virtual origin of the mixing layer is located upstream of the splitter plate apex. The development of the mixing layer width as predicted by Eq. (14) is in fair agreement with the measurements, Fig. 5. Note that no fitted function with an empirical value of S_c is needed, as proposed by Chu and Babarutsi.[1] According to Eq. (14), the mixing layer width will reach its maximum value at $x\to\infty$.

Due to the deceleration of the high velocity side and the acceleration of the low velocity side, the center of the mixing
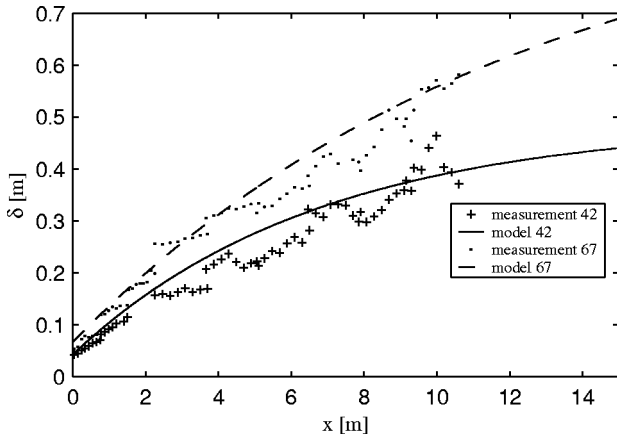
FIG. 5. The measured and modeled [Eq. (14)] development of the mixing layer width for the 42 and 67 mm cases.

layer is displaced in the lateral direction to the low velocity side. To estimate this lateral shift, the center of the mixing layer is assumed to be a streamline of the mean flow field. An integral mass balance can then be derived for as an example, the high velocity side:

$$\int_0^{y_c(x)} H U(x,y) dy = H \frac{W}{2} U_1(x_0) \tag{15}$$

from which y_c is solved. The predicted shift of the center of the mixing layer is compared with the measurements in Fig. 6. Again, the agreement is satisfactory.

The mean flow field is now completely determined by Eqs. (8), (9), (12), (14), and (15) and the boundary conditions, i.e., the two inflow velocities and the water depth. The only empirical parameter used is the entrainment coefficient α, for which the empirical value determined from unbounded mixing layers is used. The value of c_f is well defined for fully developed flows over smooth surfaces. Figure 7 shows an overview of the measured and modeled mean streamwise velocity for the 67 mm case. The model predicts the measured flow field rather well and the results are considered suitable as input for the stability analysis.
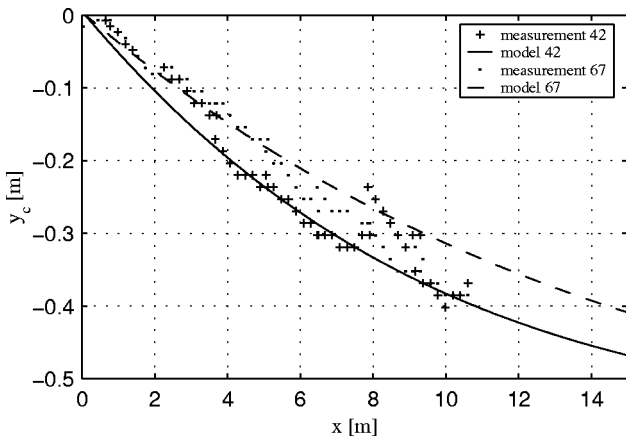

FIG. 6. Development of the measured and modeled transverse position of the center of the mixing layer for the 42 and 67 mm cases.
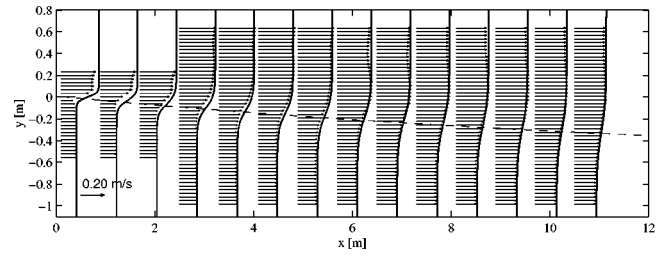

FIG. 7. Velocity vectors (measurements) and profiles (model) of the mean velocity field of the 67 mm case. The dashed line indicates the position of the center of the mixing layer.

C. Stability analysis

1. Model description

A straightforward linear stability analysis for shallow water flows has been carried out by various authors.[3–5] Comparison of linear stability analyses with measurements is however scarce, although a first successful comparison of the typical wave number in a compound channel flow was made by Tamai et al.[12] The equations for the stability analysis are equal to the ones of Alavian and Chu,[3] but differ slightly from the analyses of Chu et al.[5] and Chen and Jirka.[4,13] A short description of the model is therefore given in the following.

The shallow water equations (2)–(4) are used as starting point. In contrast with the analysis by Chu et al.,[5] the viscosity term is maintained here. Chen and Jirka[4] have demonstrated the importance of the turbulence viscosity since it affects the stability of the flow.

Following the common approach of linear stability analysis, small perturbations are superposed on the mean velocity and water level:

$$\tilde{u} = U(x,y) + u(x,y,t), \quad \tilde{v} = v(x,y,t),$$
$$\tilde{h} = H + h(x,y,t). \tag{16}$$

Reynolds decomposition of the shallow water equations (2)–(4) results in equations for the perturbations. The low Froude numbers (<0.5) allow for the use of the rigid lid assumption,[14] through which the fluctuations in water level h are now expressed as pressure fluctuations p. Dropping the higher order terms, this leads to

$$\frac{\partial u}{\partial x} + \frac{\partial v}{\partial y} = 0, \tag{17}$$

$$\frac{\partial u}{\partial t} + U\frac{\partial u}{\partial x} + v\frac{\partial U}{\partial y} = -\frac{\partial p}{\partial x} - \frac{c_f U}{H} u + \nu_t \left(\frac{\partial^2 u}{\partial x^2} + \frac{\partial^2 u}{\partial y^2} \right), \tag{18}$$

$$\frac{\partial v}{\partial t} + U\frac{\partial v}{\partial x} + v\frac{\partial v}{\partial y} = -\frac{\partial p}{\partial y} - \frac{c_f U}{2H} v + \nu_t \left(\frac{\partial^2 v}{\partial x^2} + \frac{\partial^2 v}{\partial y^2} \right). \tag{19}$$

The second term on the right-hand side of Eqs. (18) and (19) is obtained from a first-order Taylor expansion of the bottom friction contribution. It should be noted here that the bottom friction term obtained by Chen and Jirka[4,13] is a factor 2 larger than the one in Eq. (19).

A normal mode solution of the form $[u,v,p] = [\hat{u}(y),\hat{v}(y),\hat{p}(y)]\exp[i(kx-\omega t)]$ has been applied, in which k and ω are the respective complex wave number and frequency. Substitution of the normal mode solution into (17)–(19) results in

$$ik\hat{u}+\hat{v}'=0, \tag{20}$$

$$-i\omega\hat{u}+ikU\hat{u}+\hat{v}U'=-ik\hat{p}-\frac{c_f U}{H}\hat{u}+\nu_t(\hat{u}''-k^2\hat{u}), \tag{21}$$

$$-i\omega\hat{v}+ikU\hat{v}=-\hat{p}'-\frac{c_f U}{2H}\hat{v}+\nu_t(\hat{v}''-k^2\hat{v}). \tag{22}$$

The prime denotes the differentiation with respect to the lateral coordinate y. The set of equations (20)–(22) can be reduced by elimination of $\hat{u}$ and $\hat{p}$ to

$$\left(U-\frac{\omega}{k}\right)(\hat{v}''-k^2\hat{v})-\hat{v}U''=D_{\mathrm{bf}}+D_{\mathrm{vis}} \tag{23}$$

with

$$D_{\mathrm{bf}}=i\frac{c_f U}{kh}\left(-\frac{1}{2}k^2\hat{v}+\frac{U'}{U}\hat{v}'+\hat{v}''\right),$$

$$D_{\mathrm{vis}}=i\frac{\nu_t}{k}(\hat{v}'''-2k^2\hat{v}''+k^4\hat{v}).$$

The form of this equation is similar to the Orr–Sommerfeld equation.[15] The terms on the right-hand side, however, are different. The first term denotes the stabilizing influence of the bottom shear stress and the second term the stabilizing influence of the turbulence viscosity. The viscosity term differs from the viscosity term in the Orr–Sommerfeld equation by the use of an eddy viscosity that represents the small scale turbulence instead of the molecular viscosity. The bottom friction term is a consequence of the depth-and-short-time averaged vertical shear, and is always stabilizing as follows directly from Eqs. (21) and (22). The eigenvalue problem [Eq. (23)] can be solved by following a spatial approach or a temporal approach. The spatial approach assumes an exponential growth of the perturbations in downstream direction x. The frequency of the disturbance ω is therefore real, and k is complex, with k_r representing the wave number and k_i the spatial growth rate. The temporal approach assumes the disturbances to grow exponentially in time. In that case k is real and ω complex, with ω_i representing the temporal growth rate:

$$[u,v,p]=[\hat{u}(y),\hat{v}(y),\hat{p}(y)]\exp[i(kx-(\omega_r+i\omega_i)t)].$$

As shown by Michalke[16] the spatial approach covers the physical phenomenon of a spatial mixing layer slightly more precisely than the temporal approach. However, the eigenvalue problem of the spatial approach is more complicated to solve than the eigenvalue problem of the temporal approach, due to the nonlinearity in k. For this study we have chosen to solve the temporal eigenvalue problem instead of the spatial one. The wave number is therefore real and will be denoted without a subscript $k=k_r$, unless defined differently. The temporal approach is allowed since the length scale over
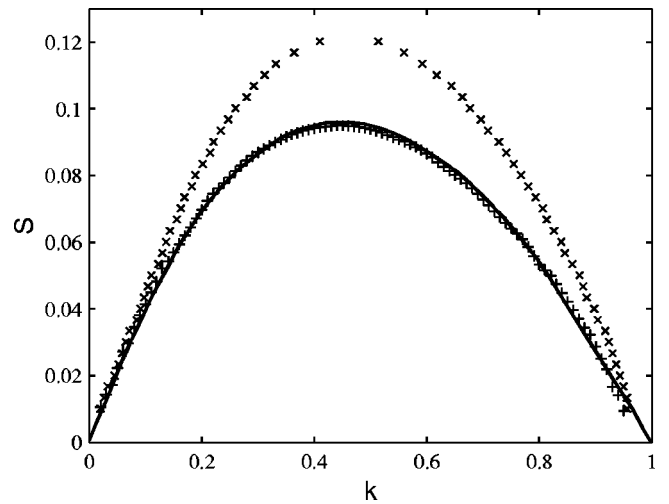

FIG. 8. Neutral stability curves of an inviscid flow obtained with Eq. (23) with the correct ($\times$) and erroneous ($+$) bottom friction term and the result by Chen and Jirka—Ref. 4 ($-$).

which the growth takes place is much larger than the length scale of the perturbations. A comparison of the temporal method with a spatial method[4] will be made in the following. According to Gaster,[17] the spatial growth rate k_i^S can easily be determined from the temporal growth rate ω_i^T by $k_i^S = \omega_i^T/c^T$ with $c^T=\omega_r^T/k^T$ as the propagation velocity.

The eigenvalue problem of Eq. (23) is solved for given wave numbers yielding the growth rate ω_i and frequency ω_r, by using a finite difference technique. The stability of the flow follows from the stability curves $(k,\omega_i(k))$. Perturbations with wave number k are growing if $\omega_i(k)>0$. In order to validate the proposed temporal method for the linear stability analysis, a comparison is made with the inviscid calculations of Chen and Jirka,[4] who solved the eigenvalue problem with the spatial method. Stability curves are therefore calculated for a range of profiles, determined by a bed friction number S [Eq. (1)]. The zero crossings of these curves determine the neutral stability curve, which is chosen as the criterion for comparison. The neutral stability curves determine the critical wave numbers where $\omega_i(k)=0$. Figure 8 shows three different neutral stability curves. The first curve is the neutral stability curve according to the above-described model, and the second is obtained from Chen and Jirka.[4] The large difference between these curves can be ascribed to the incorrect derivation of the bottom friction term in the eigenvalue problem of Chen and Jirka.[4] Implementation of the erroneous bottom friction term into the current model results in the third curve, which coincides with the original curve of Chen and Jirka.[4] With this comparison the use of the temporal approach instead of the spatial approach is justified. In subsequent sections the above-described linear stability analysis model is used. For sensitivity analyses regarding bottom friction and eddy viscosity we refer to Chen and Jirka.[4]

2. Experimental validation

The above-described stability analysis is applied to the experiments of Sec. II. The validated velocity profiles, com-

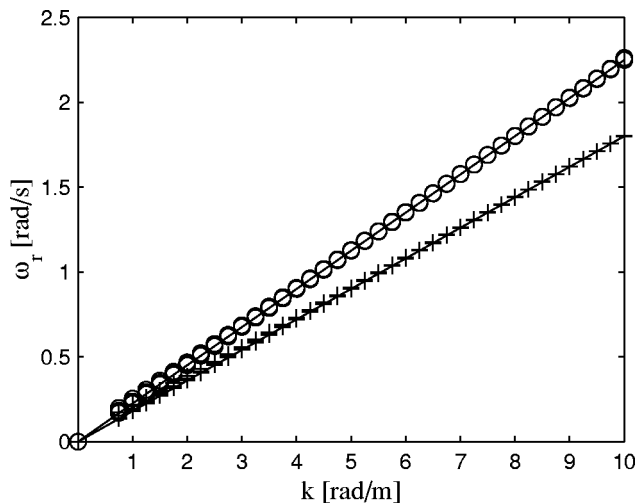FIG. 9. Dispersion relation for the 42 mm case ($+$) and the 67 mm case ($\bigcirc$). The solid lines represent kU_c.

puted with the one-dimensional-model of Eq. (8), are used as base flow. Stability curves are determined for a number of positions downstream of the splitter plate up to a length of 15 m. In Fig. 9 the determined frequencies ω_r are shown versus k. The frequencies are linearly proportional to the wave numbers with a proportionality constant equal to the velocity at the center of the mixing layer, justifying the use of the temporal method again.

Figure 10 shows the growth rates at several positions downstream of the splitter plate for both mixing layers. A positive value of the growth rate indicates growth of the perturbation of the particular wave number and a negative value indicates decay of that mode. For each position downstream, a maximum growth rate is found, determining the locally most unstable mode. The wave number of this unstable mode is close to $k \simeq 0.445/(0.5\delta)$ as found by Michalke.[18] The most unstable mode is therefore proportional to the mixing layer width. The wave number of this most unstable mode decreases in downstream direction as a
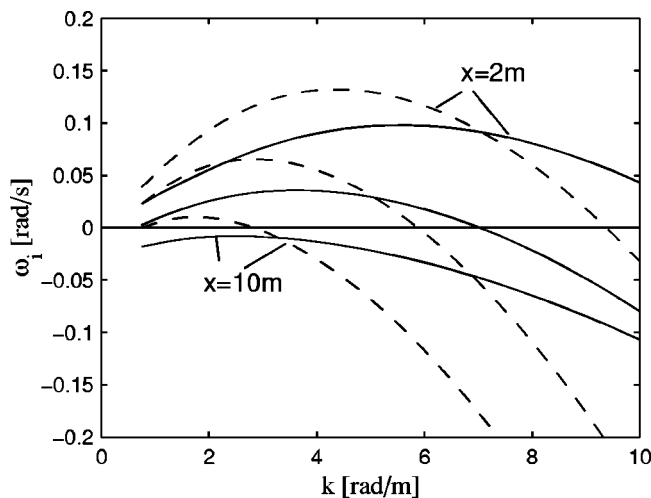
consequence of the broadening of the mixing layer width. The wave number of the most unstable mode is decreasing more rapidly for the 67 mm case than for the 42 mm case as the mixing layer width is growing faster for the 67 mm case. The magnitude of the growth rate also decreases in downstream direction. This decrease in magnitude is stronger for the 42 mm case than for the 67 mm case. The dissipative influence of the bottom friction is the same for each wave number, as directly follows from Eqs. (21) and (22). Note that the influence of the bottom friction is also implicitly present in the decrease of the mean velocity difference. The dissipation due to the turbulence viscosity is proportional to k^2, thus affecting the modes with large wave numbers stronger than the modes with small wave numbers. Comparing the two cases shows that the growth rates of the modes with small wave numbers are larger for the 67 mm case than for the 42 mm case, because the influence of the bottom friction is smaller for the deeper 67 mm case. The growth rates of the modes for the large wave numbers are more strongly influenced by the eddy viscosity, resulting in smaller growth rates for the 67 mm case than for the 42 mm case in the high wave number range. In the case with bottom friction and/or viscosity, the dissipative terms can become larger than the production terms, resulting in a negative growth rate. For these cases existing disturbances are being dissipated, the stable situation is reached, as for example for the 42 mm case at $x = 10$ m.

The stability curves of Fig. 10 represent the growth rate for the various wave numbers at a given downstream position, but they do not predict the energy density of the wave numbers at that particular position. In order to find this energy density, the history of the development of the structures has to be taken into account. Integrating the growth rates over the streamwise coordinate yields an amplification factor for the initial perturbation. The energy density spectrum, of the lateral velocity component, for a certain position downstream x_1 is then determined by

$$E(k,x_1) = E(k,x_0) \int_{x_0}^{x_1} \exp\left(\frac{\omega_i(k)}{\omega_r(k)} kx \right) dx. \qquad (24)$$

The initial spectrum denoted by $E(k,x_0)$ is assumed to be that of an undisturbed open channel flow. Such a spectrum is flat for small wave numbers. The initial energy density level is taken such that it equals the measured energy density at a position just downstream of the splitter plate, Fig. 11. The resulting spectra at several positions, which are obtained by discretization of Eq. (24), are plotted in Figs. 11(a) and 11(b) for the 42 mm case and the 67 mm case, respectively. The measured energy density spectra of the lateral velocity obtained in the center of the mixing layer are also plotted in Fig. 11, showing a remarkably good agreement. Since the measured spectra are obtained from time series, the frequency axes are converted to wave numbers by using the propagation velocity.

The presence of large coherent structures is reflected in a significant peak in the spectra. Moving in downstream direction, the wave number of the peak shifts to the low wave number side, corresponding to an enlargement of the struc-
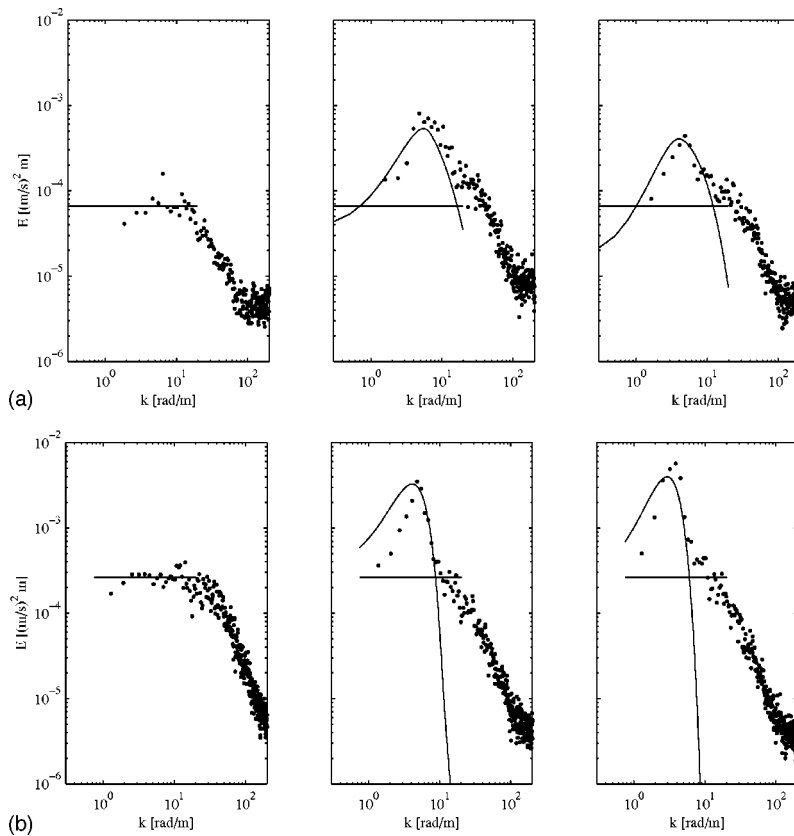

FIG. 10. Stability curves for the 42 mm case (solid) and the 67 mm case (dashed) for different positions downstream ($x = 2$, 4.5, and 10 m).

FIG. 11. Measured (dots) and modeled (solid line) energy density spectra of the lateral velocity component v for the 42 mm case (a) and the 67 mm case (b) in the center of the mixing layer at the downstream positions $x=0$, 4.5, and 10 m.

tures. The energy density of the peak is growing for the 67 mm case over the full stretch, yielding intenser vortices. The peak in the spectrum of the 42 mm case at $x=10$ m is, however, lower than the one at $x=4.5$ m, indicating a decrease in strength for the large coherent structures.

Although the linear stability analysis is used here beyond its limits of small perturbations, and the growth rates are integrated over a stretch several times the length scale of the perturbations, the analysis gives a good prediction of the energy density and the typical wave number of the coherent structures. The high wave number range of the spectrum, which is influenced by the dissipative small scale motion, is underestimated. Obviously Eq. (6) does not fully apply to this range of the spectrum, because the small scale three-dimensional motion in this range is not resolved in this analysis. The successful prediction using a linear analysis suggests that the coherent structures are hardly influencing each other and that the energy density spectrum at a certain position downstream is governed by the spectral distribution of the turbulent kinetic energy at the inflow boundary.

In order to track the development of the large coherent structures, the dominant mode is followed. The dominant mode is defined as the wave number associated with the maximum energy density and is therefore representing the large coherent structures. As mentioned earlier, the most unstable mode is the wave number for which the energy is growing fastest. A more sophisticated way to identify the coherent structures and their evolution from the measurements is by conditional averaging, see, for example, Scarano et al.[19] In this study however, we restrict ourselves to the development of the dominant mode, since this property is

obtained from the stability analysis as well as from the experiments.

The growth in intensity of the coherent structures is determined in downstream direction by following the growth rate of the dominant mode. The growth rates ω_i of the dominant modes are plotted as function of the downstream position x in Fig. 12. At a certain position downstream, the growth rate of the dominant mode becomes zero indicating that from that position on the coherent structures are losing energy. The coherent structures are still present, but are decaying. An unstable mode with positive growth rate can,
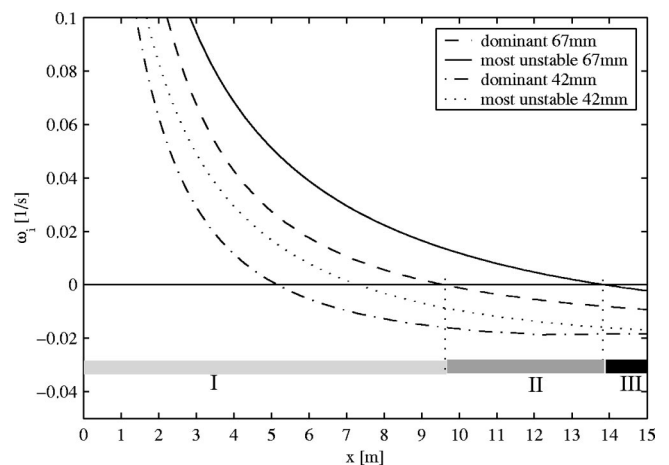

FIG. 12. Development of the growth rates of the most unstable modes and the dominant modes for the 42 and 67 mm cases. The three different growth regimes are indicated for the 67 mm case.
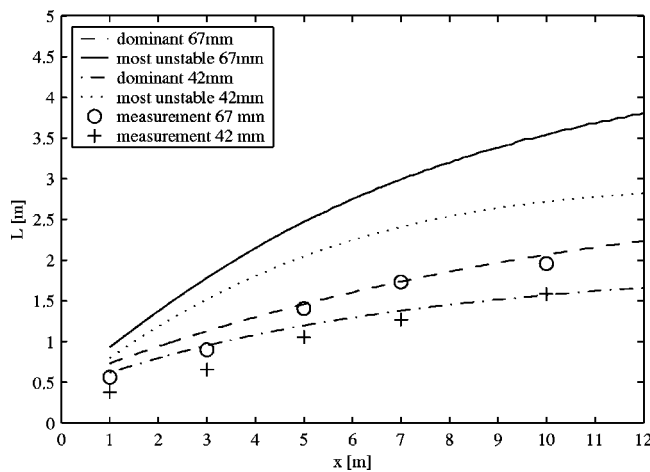
FIG. 13. Development of the length scale of the most unstable mode, the dominant mode, and the measured dominant mode for the 42 and 67 mm cases.
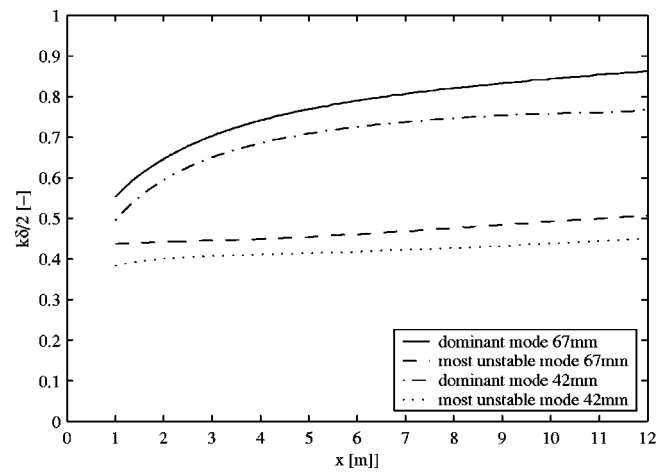

FIG. 14. Development of the dimensionless wave number $k^* = k\delta/2$ of the most unstable mode and the dominant mode for the 42 and 67 mm cases.

however, still be found up to the downstream position where the most unstable mode has a growth rate equal to zero. From that position on the flow is stable and all perturbations will decay. At this position the bottom friction parameter has reached its critical value,[3] $S = S_c$.

Three different regimes can now be distinguished (see Fig. 12). The first regime (I) is characterized by the positive growth rate of the dominant mode. In the second regime (II) the growth rate of the dominant mode is negative (the coherent structures are decaying), while some other modes still have positive growth rates. The flow is therefore not stable yet. The third regime (III) is the stable regime, where all modes are dissipating and the growth rates are negative. Although the flow is stable, coherent structures still might exist in this stable regime. As these large perturbations have a small wave number k, they are hardly influenced by the turbulence viscosity. Therefore, an exponential decay of the energy content due to effects of bottom friction is expected beyond this point.

The development in downstream direction of the characteristic length scale associated with the coherent structures is related to the wave number of the dominant mode and can be determined from the modeled and measured spectra. The time scale of the dominant mode is determined by the frequency of the peak in the spectrum. Multiplying this time scale by the propagation velocity results in the length scale of the dominant mode. The development of these measured and modeled length scales is plotted in Fig. 13 together with the development of the length scales of the most unstable modes. As demonstrated in Fig. 11, the modeled and measured length scales of the dominant modes are in good agreement. As Fig. 13 shows, the length scale of the most unstable mode is much larger than the length scale of the dominant mode. The coherent structures generated upstream have had the opportunity to grow in strength while being advected downstream. The effect of the advection is made more clear in Fig. 14 by the dimensionless wave number $k^* = k\delta/2$ as also used by Michalke.[18] The wave number of the most unstable mode is almost constant and close to the value of k^*

$\simeq 0.445$.[5,18] The wave number of the dominant mode is, however, not constant, but changes in downstream direction as the advection of the coherent structures play a role. The wave number found far downstream is about twice as large as the wave number of the most unstable mode.

The determination of the most unstable mode is therefore not suitable for characterization of the large scale motion. It highly overestimates the size of the coherent structures. The accumulated energy of the coherent structures has to be taken into account for the determination of the typical length scale using the dominant mode instead of the most unstable mode.

IV. CONCLUSIONS

This study demonstrates that with relatively simple techniques and means, a detailed view can be obtained on the shallow mixing layer and its large scale structures.

The quasi-1-D model predicts a mean flow field in accordance with the measured flow field. The validity of the model suggests that the effects of shallowness on the mean flow field are mainly governed by the decrease of the velocity difference over the mixing layer as a result of bottom friction. The contribution of small scale three-dimensional turbulence to the growth rate of the mixing layer and the associated entrainment appears to be negligible. Only at downstream locations where Reynolds stresses in the horizontal plane have become of the same order of magnitude as those in the vertical plane, a change in the entrainment coefficient α could be expected.

The use of a mean flow field as a base flow gives an extension to the use of linear stability analysis. In contrast with the classical analysis based on a single velocity profile for which the growth rates and the most unstable mode are determined at a single location, the use of a flow field here allows for the determination of the spatial evolution of the energy densities and the characteristic length scales. The development of the growth rate of the dominant mode shows that the flow "stabilizes" (i.e., the dominant mode decays) well before the critical bottom friction number is reached $S = S_c$, where all modes decay. The critical bottom friction

number is therefore not a useful number to characterize the large scale motion as proposed in Chu and Babarutsi.[1] Although the linear stability analysis is used beyond its limits, the characteristics of the large scale motion are well predicted. This implies that the different modes hardly influence each other. A nonlinear analysis is expected to yield a more strict criterion as to the extent to which the linear approach is justified.

A consequence of the linear behavior is that the spectral distribution of perturbations at the inflow boundary is determining the intensity of the coherent motion further downstream. Numerical simulations resolving the coherent motion and modeling the small scale motion are therefore expected to be very sensitive to the perturbations prescribed at the inflow boundary.

This study has provided good insight into the dynamical processes in a shallow mixing layer, which are important for the transverse exchange of mass and momentum. The combined model can be used as a quick tool to predict the characteristics of coherent structures that are to be found in laboratory experiments and in the field. Further extensions like variations in depth and bottom roughness should be made to provide wider applications in environmental fluid mechanics.

ACKNOWLEDGMENTS

[1] V. H. Chu and S. Babarutsi, "Confinement and bed-friction effects in shallow turbulent mixing layers," J. Hydraul. Eng. **114**, 1257 (1988).

[2] W. S. J. Uijttewaal, D. Lehmann, and A. van Mazijk, "Exchange processes between a river and its groyne fields: Model experiments," J. Hydraul. Eng. **127**, 928 (2001).

[3] V. Alavian and V. H. Chu, "Turbulent exchange flow in shallow compound channel," 21st IAHR Congress, Melbourne, 1985, pp. 446–451.

[4] D. Chen and G. H. Jirka, "Linear stability analysis of turbulent mixing layers and jets in shallow water layers," J. Hydraul. Eng. **36**, 815 (1998).

[5] V. H. Chu, J. H. Wu, and R. E. Khayat, "Stability of the transverse shear flow in shallow open channels," J. Hydraul. Eng. **117**, 1371 (1989).

[6] T. Dracos, M. Giger, and G. H. Jirka, "Plane turbulent jets in a bounded fluid layer," J. Fluid Mech. **214**, 587 (1992).

[7] W. S. J. Uijttewaal and R. Booij, "Effects of shallowness on the development of free-surface mixing layers," Phys. Fluids **12**, 392 (2000).

[8] R. J. M. Bastiaans, G. A. J. van der Plas, and R. N. Kieft, "The performance of a new PTV algorithm in super-resolution PIV," Exp. Fluids **32**, 346 (2002).

[9] H. B. Fischer, E. J. List, R. C. J. Koh, J. Imberger, and N. H. Brooks, *Mixing in Inland and Coastal Waters* (Academic, New York, 1979).

[10] A. A. Townsend, *The Structure of Turbulent Shear Flow* (Cambridge University Press, Cambridge, 1956).

[11] M. Lesieur, *Turbulence in Fluids* (Kluwer Academic, Dordrecht, 1997).

[12] N. Tamai, T. Aseada, and H. Ikeda, "Study on generation of periodical large surface eddies in a composite channel flow," Water Resour. Res. **22**, 1129 (1986).

[13] D. Chen and G. H. Jirka, "Absolute and convective stabilities of plane turbulent wakes in a shallow water layer," J. Fluid Mech. **338**, 157 (1997).

[14] M. S. Ghidaoui and A. A. Kolyshkin, "Linear stability analysis of lateral motions in compound open channels," J. Hydraul. Eng. **125**, 871 (1999).

[15] P. G. Drazin and W. H. Reid, *Hydrodynamic Stability* (Cambridge University Press, Cambridge, 1981).

[16] A. Michalke, "On spatially growing disturbances in an inviscid shear layer," J. Fluid Mech. **23**, 521 (1965).

[17] M. Gaster, "A note on the relation between temporally-increasing and spatially-increasing disturbances in hydrodynamic stability," J. Fluid Mech. **14**, 222 (1962).

[18] A. Michalke, "On the inviscid instability of the hyperbolic-tangent velocity profile," J. Fluid Mech. **19**, 543 (1964).

[19] F. Scarano, C. Benocci, and M. L. Riethmuller, "Pattern recognition analysis of the flow past a backward facing step," Phys. Fluids **11**, 3808 (1999).